ELSEVIER

Contents lists available at ScienceDirect

Earth and Planetary Science Letters

journal homepage: www.elsevier.com/locate/epsl



Mercury isotope evidence for recurrent photic-zone euxinia triggered by enhanced terrestrial nutrient inputs during the Late Devonian mass extinction



Wang Zheng ^a, Geoffrey J. Gilleaudeau ^{b,*}, Thomas J. Algeo ^{c,d}, Yaqiu Zhao ^a, Yi Song ^e, Yuanming Zhang ^a, Swapan K. Sahoo ^f, Ariel D. Anbar ^{g,h}, Sarah K. Carmichael ⁱ, Shucheng Xie ^j, Cong-Qiang Liu ^a, Jiubin Chen ^{a,*}

- ^a School of Earth System Science, Institute of Surface-Earth System Science, Tianjin University, 300072 Tianjin, China
- ^b Department of Atmospheric, Oceanic, and Earth Sciences, George Mason University, Fairfax, VA 22030, USA
- ^c Department of Geosciences, University of Cincinnati, Cincinnati, OH 45221-0013, USA
- d State Key Laboratories of BGEG and GPMR, China University of Geosciences, School of Earth Sciences, Wuhan 430074, China
- ^e Guangxi Laboratory on the Study of Coral Reefs in the South China Sea, Coral Reef Research Center of China, School of Marine Sciences, Guangxi University, Nanning. 530004. PR China
- f Equinor US, Houston, TX, USA
- ^g School of Earth and Space Exploration, Arizona State University, Tempe, AZ 85287, USA
- ^h School of Molecular Sciences, Arizona State University, Tempe, AZ 85287, USA
- i Department of Geological and Environmental Sciences, ASU Box 32067, Appalachian State University, Boone, NC 28608, USA
- ^j State Key Laboratory of Biogeology and Environmental Geology, China University of Geosciences, School of Earth Sciences, Wuhan 430074, China

ARTICLE INFO

Article history: Received 16 January 2023 Received in revised form 7 April 2023 Accepted 18 April 2023 Available online 10 May 2023 Editor: A. Jacobson

Keywords:
mercury isotopes
photic zone euxinia
Frasnian-Famennian boundary
Devonian-Carboniferous boundary
Kellwasser
Hangenberg

ABSTRACT

Widespread oceanic anoxia marked by globally extensive deposition of organic-rich black shale during the Late Devonian was a major factor in the mass extinctions at the Frasnian-Famennian (FFB, \sim 372 million years ago) and Devonian-Carboniferous boundaries (DCB, \sim 359 million years ago), although the triggers for these deoxygenation events are still under debate. Here, we apply a novel paleoredox proxy, Hg isotopes, to investigate Late Devonian ocean redox variation and its causes. We found no Hg enrichments in North America across either the FFB or DCB, thus arguing against the hypothesis of global-scale volcanism as the trigger for Late Devonian environmental and biotic crises. Gradual negative shifts of both mass-independent fractionation (Δ^{199} Hg) and mass-dependent fractionation (δ^{202} Hg) occurred between the FFB and DCB, suggesting a progressive increase of Hg inputs associated with terrestrial organic matter. Moreover, multiple abrupt negative excursions of Δ^{199} Hg (down to -0.19%) along with concurrent positive shifts of δ^{202} Hg occurred just above the FFB and across the DCB, providing strong evidence for recurrent photic-zone euxinia (PZE) that was preceded by increasing terrestrial inputs in the epicontinental seas of North America. We suggest that the increase of terrestrial inputs of nutrients, probably via expansion of vascular land plants, stimulated marine primary productivity and eventually PZE, which may have been a key kill mechanism for the Late Devonian mass extinction.

© 2023 Elsevier B.V. All rights reserved.

1. Introduction

The Late Devonian (\sim 383-359 Ma) was marked by several extinction episodes, collectively representing one of the "Big Five" mass extinctions in Earth history with a 70-82% extinction rate among marine invertebrate species (Sallan and Coates, 2010).

The two largest extinction pulses occurred close to the Frasnian-Famennian boundary (FFB, ~372 Ma) (Percival et al., 2018a) and the Devonian-Carboniferous boundary (DCB, ~359 Ma) (Kaiser et al., 2016). These extinctions were associated with strong environmental perturbations, including large-scale volcanism (Racki et al., 2018; Racki, 2020; Kaiho et al., 2021), eustatic fluctuations (Johnson et al., 1985), long-term increases of continental weathering due to the expansion of terrestrial plants (Algeo et al., 1995; Algeo and Scheckler, 1998) or tectonic activity (Averbuch et al., 2005), possible increases in UV radiative flux (Marshall et al., 2020), and widespread oceanic anoxia/euxinia (Caplan and Bustin, 1999;

^{*} Corresponding authors.

E-mail addresses: ggilleau@gmu.edu (G.J. Gilleaudeau), jbchen@tju.edu.cn
(J. Chen).

Marynowski et al., 2012; Liu et al., 2019; Song et al., 2021; Zhang et al., 2020; Sahoo et al., 2023). However, the roles of these processes as drivers of Late Devonian mass extinction are still under debate.

Oceanic anoxia has long been regarded as a potent kill mechanism during mass extinctions (Algeo et al., 1995; Bond and Grasby, 2017). Widespread anoxia during the Late Devonian is documented by globally extensive deposition of organic-rich black shale around the FFB (Lower and Upper Kellwasser Events) and DCB (Hangenberg Event) (Caplan and Bustin, 1999; Algeo et al., 2007; Marynowski et al., 2012; Carmichael et al., 2019; Liu et al., 2019). These black shales offer abundant evidence of watercolumn anoxia or euxinia (i.e., sulfide-rich conditions) in the form of various organic (e.g., lipid biomarker) and inorganic proxies (e.g., redox-sensitive trace elements, pyrite framboids, metal isotopes) (Marynowski et al., 2012; Paschall et al., 2019; Kabanov and Jiang, 2020; Song et al., 2021). Moreover, contemporaneous photic-zone euxinia (PZE) has been widely documented in epicontinental and continental-margin settings (Kabanov and Jiang, 2020; Song et al., 2021) based on lipid biomarkers of anoxygenic photoautotrophs (e.g., green and brown sulfur bacteria). The occurrence of PZE is particularly detrimental to shallow-marine organisms and is proposed to have been a direct kill mechanism for most or all of the "Big Five" mass extinction events (Whiteside and Grice, 2016). However, the ultimate trigger of widespread anoxia and PZE during the Late Devonian is not yet clear.

Recently, the use of Hg chemostratigraphy in sedimentary successions has facilitated investigation of the role of large igneous provinces (LIPs) in major environmental and biotic crises in Earth history. Large-scale LIP eruptions frequently result in widespread Hg enrichment (i.e., Hg anomalies) in marine and terrestrial facies (Percival et al., 2017; Grasby et al., 2019). Massive volcanism can trigger many environmental changes that are potential proximal kill mechanisms during mass extinctions, including oceanic anoxia (Bond and Grasby, 2017). All of the "Big Five" mass extinction events have been linked to LIPs to some degree, including the Kellwasser and Hangenberg crises (Bond and Grasby, 2017; Racki, 2020). However, some of the Late Devonian biotic crises (e.g., the Hangenberg Crisis) do not have a geological record of contemporaneous LIPs (Racki, 2020). Moreover, Hg anomalies in sedimentary rocks can also be produced by non-LIP processes, such as submarine hydrothermal emissions, terrestrial soil erosion, and biomass burning, or through sequestration of seawater Hg under anoxic/euxinic conditions (Them et al., 2019; Shen et al., 2019). Thus, the links between LIPs, oceanic anoxia, and mass extinctions during the Late Devonian remain uncertain.

Mercury isotopes in sedimentary rocks have the potential to provide new insights into the links between environmental crises and mass extinctions. In modern environments, Hg isotopes have been widely used as a powerful tracer of Hg sources and transformations (Blum et al., 2014; Kwon et al., 2020), owing to the unique advantage that Hg isotopes exhibit both mass-dependent (MDF) and mass-independent fractionation of both odd (odd-MIF) and even (even-MIF) mass number isotopes. In ancient marine environments, Hg isotopes have been successfully applied to distinguish between volcanic versus non-volcanic Hg sources to the ocean (Thibodeau et al., 2016; Grasby et al., 2017, 2019; Them et al., 2019). Moreover, Hg isotopes have been recently recognized as a promising proxy for PZE (Zheng et al., 2018). Our previous study of Hg isotopes in the Mesoproterozoic ocean found that sedimentary rocks deposited under PZE exhibit more negative odd-MIF and more positive MDF than those formed under non-PZE conditions. This observation was explained by two possible mechanisms: photoreduction of Hg(II) complexed by reduced sulfur in a sulfide-rich photic zone, and enhanced sequestration of atmospheric Hg(0) by sulfidic surface water. Both mechanisms can lead to the observed shifts of Hg isotopes under PZE, as supported by multiple experimental studies (Zheng and Hintelmann, 2010; Zheng et al., 2019).

Here, we present a high-resolution dataset of Hg concentrations and isotopes for a black shale succession from Tennessee (United States, North America) that spans the full Upper Devonian. Together with published biostratigraphic (Over et al., 2019) and multiproxy data (i.e., iron speciation, redox-sensitive trace elements, organic biomarkers) for this section (Song et al., 2021), our study provides strong evidence for recurrent PZE during extinction events of the Late Devonian. It also sheds new light on the relationship of PZE to volcanism and enhanced terrestrial erosion, thus allowing further evaluation of the impacts of land plants and ocean redox changes on the Late Devonian mass extinctions.

2. Geological setting

Our study section is a drillcore (Dupont GHS) collected by the Dupont Chemical Corporation from Humphreys County, Tennessee (36.13°N, 87.83°W). This core contains the Chattanooga Shale and the base of the overlying Maury Shale, providing a high-resolution record of nearly the full Upper Devonian, including the FFB and DCB, and the lowermost Mississippian. The paleogeographic location of the study site is within the North American Devonian Seaway (Algeo et al., 2007), on the shallow Cumberland Sill separating the semi-restricted epicratonic Illinois and Appalachian basins from the open Rheic Ocean to the south (Fig. 1). The paleogeography, sedimentology, conodont biostratigraphy, and paleoenvironments of the study core have been described in detail in earlier studies (Over et al., 2019; Over, 2020; Song et al., 2021). The majority of the study units are comprised of organic-rich, black, laminated shale with no visible evidence for bioturbation or benthic fossils. The base of the Chattanooga Shale (0 m in the study core) rests on a disconformity above the Givetian-age Sellersburg Formation. The FFB is present at a disconformity at 4.7 m. The DCB is within a gray shale interval at 13.5-14.0 m that contains no conodont fossils but abundant phosphate nodules (Song et al., 2021). This non-fossiliferous interval spans six conodont zones from the top of the upper Famennian aculeatus Zone to the lower Tournaisian sandbergi Zone and contains a disconformity at the Chattanooga-Maury Formation contact (Over et al., 2019). The Dasberg Event, a smaller extinction that preceded the Hangenberg Event, coincided with the aculeatus Zone, but the Hangenberg Event itself is either missing or represented by non-fossiliferous

3. Analytical methods

3.1. Hg concentration analysis

Hg concentrations in rock samples were analyzed by a Lumex RA-915F Hg Analyzer equipped with a thermal pyrolysis unit (Lumex, St. Petersburg, Russia) at Tianjin University. Hg in samples was released as Hg(0) vapor by pyrolysis at a temperature of \sim 750°C, and then measured by cold vapor atomic absorption spectroscopy (CV-AAS). A certified reference material GBW07311 (GSD-11, freshwater sediment) was measured repeatedly along with samples to ensure the accuracy and reproducibility of the analysis. The GSD-11 standard material gave an average Hg concentration of 72.0 \pm 7.4 ng·g⁻¹ (2SD, n = 6), which is consistent with the certified value 72 \pm 9 ng·g⁻¹.

3.2. Hg isotope analysis

Before Hg isotope analysis, total Hg in rock samples was extracted using a pyrolysis method (see details in Supplementary Text S1). Four certified reference materials, SBC-1 (Brush Creek

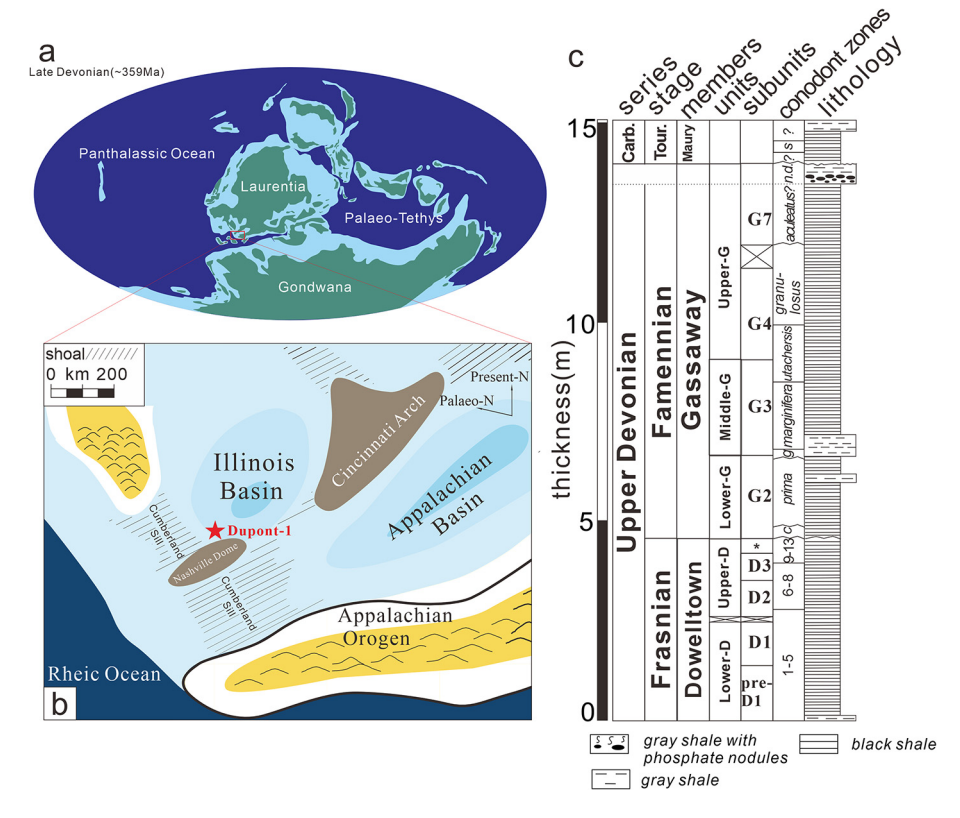


Fig. 1. Paleogeographic map of the study location and generalized stratigraphy of the Chattanooga Shale (modified from Song et al., 2021). (a) Global geographic map of the Late Devonian (\sim 359 Ma). (b) Details of the southern Laurentian Craton. (c) Stratigraphy of the Dupont GHS drillcore, showing conodont zones and subdivisions of the Chattanooga Shale. Abbreviations: MD = Middle Devonian, Carb. = Carboniferous, Giv. = Givetian, Tour. = Tournaisian, c = crepida, g = gracilis, s = sandbergi, Sg = Sellersburg, D = Dowelltown, G = Gassaway, and * = condensed units D4 and D5.

Shale), SCO-2 (Cody Shale), NIST SRM 2702 (marine sediments), and NIST SRM 1944 (estuarine sediments), were pyrolyzed in the same way as the samples to evaluate the recovery of the pyrolysis process and its influence on isotopic analysis. The pyrolysis blank contained less than 0.03 $\rm ng\cdot g^{-1}$ Hg (<2% of the Hg concentration of samples). The Hg recovery for all samples averaged 98 \pm 13% (2SD).

Mercury isotopes were analyzed using multi-collector inductively coupled plasma mass spectrometry (MC-ICPMS, Neptune Plus, Thermo Scientific, and Nu plasma 3D, Nu instruments Ltd.) at the School of Earth System Science, Tianjin University, following published methods (Shi et al., 2023). In short, the trapping solutions were diluted to 1 to 2 $\text{ng} \cdot \text{g}^{-1}$ of Hg. SnCl_2 solution (3%, w/v) was used to reduce Hg(II) in the trapping solutions to gaseous Hg(0), which was then carried into the plasma of the MC-ICPMS by Hg-free argon gas. At the same time, Tl aerosol (NIST SRM 997) generated by a nebulizer device (Aridus II) was also introduced together with Hg(0) vapor into the plasma. Six Hg isotopes (198 Hg, 199 Hg, 200 Hg, 201 Hg, 202 Hg, 204 Hg) and two Tl isotopes (²⁰³Tl, ²⁰⁵Tl) were simultaneously measured by Faraday cups in the MC-ICPMS. Instrumental mass bias was corrected using ²⁰⁵Tl/²⁰³Tl ratio and standard-sample-standard bracketing with the NIST 3133 Hg standard. The bracketing standard was matched to samples in terms of both matrix and Hg concentration (less than 10% difference). Mercury isotope compositions are reported using δ notation defined by the following equation:

$$\delta^x Hg = [(^xHg/^{198}Hg)_{sample}/(^xHg/^{198}Hg)_{std} - 1] \times 1000 \tag{1}$$

where $^{\rm X}$ Hg is 199 Hg, 200 Hg, 201 Hg, 202 Hg, or 204 Hg, and the standard (std) is the NIST SRM 3133 mercury standard solution. MDF is typically represented by δ^{202} Hg. MIF is defined as the deviation

of measured δ^x Hg from theoretical mass-dependent kinetic isotope fractionation according to the following equation (Blum and Bergquist, 2007):

$$\Delta^{x} Hg = \delta^{x} Hg - (\delta^{202} Hg \times \beta)$$
 (2)

where x is the mass number of Hg isotopes 199, 200, 201, and 204, and β is a scaling constant to estimate the theoretical kinetic MDF, with a value of 0.2520, 0.5024, 0.7520, and 1.493 for ¹⁹⁹Hg, ²⁰⁰Hg, ²⁰¹Hg, and ²⁰⁴Hg, respectively.

To ensure data quality, each sample was measured at least twice, and a commonly used reference standard NIST SRM 8610 was measured every seven samples to monitor instrument performance. The averages for all analyses of NIST 8610 were: $\delta^{202} \text{Hg} = -0.52 \pm 0.09\%$, $\Delta^{199} \text{Hg} = 0.00 \pm 0.04\%$, $\Delta^{201} \text{Hg} = -0.02 \pm 0.03\%$, and $\Delta^{200} \text{Hg} = 0.01 \pm 0.04\%$ (2SD, n = 11), consistent with published values (Blum and Bergquist, 2007). The certified reference materials NIST SRM 1944 (estuarine sediments) and NIST SRM 2702 (marine sediments) yielded average δ^{202} Hg, Δ^{199} Hg, Δ^{201} Hg, and Δ^{200} Hg values of $-0.46 \pm 0.09\%$, 0.01 \pm 0.04%, $0.01 \pm 0.03\%$, $0.01 \pm 0.04\%$ (n = 4) and $-0.79 \pm 0.09\%$, $0.00 \pm 0.04\%$, $0.00 \pm 0.03\%$, $0.02 \pm 0.04\%$ (n = 5), respectively (Table S1). These values are in excellent agreement with published values (Blum and Johnson, 2017; Shi et al., 2023), demonstrating robust data quality. All isotope data are reported in Table S2, and the analytical uncertainties are given either as two standard errors (2SE) of sample replicates or as two standard deviations (2SD) of all measurements of the NIST 8610 standard (whichever is higher).

4. Results

For purposes of discussion, we subdivide the Chattanooga Shale into three units: Unit I contains the full Frasnian Stage (0 to 4.7

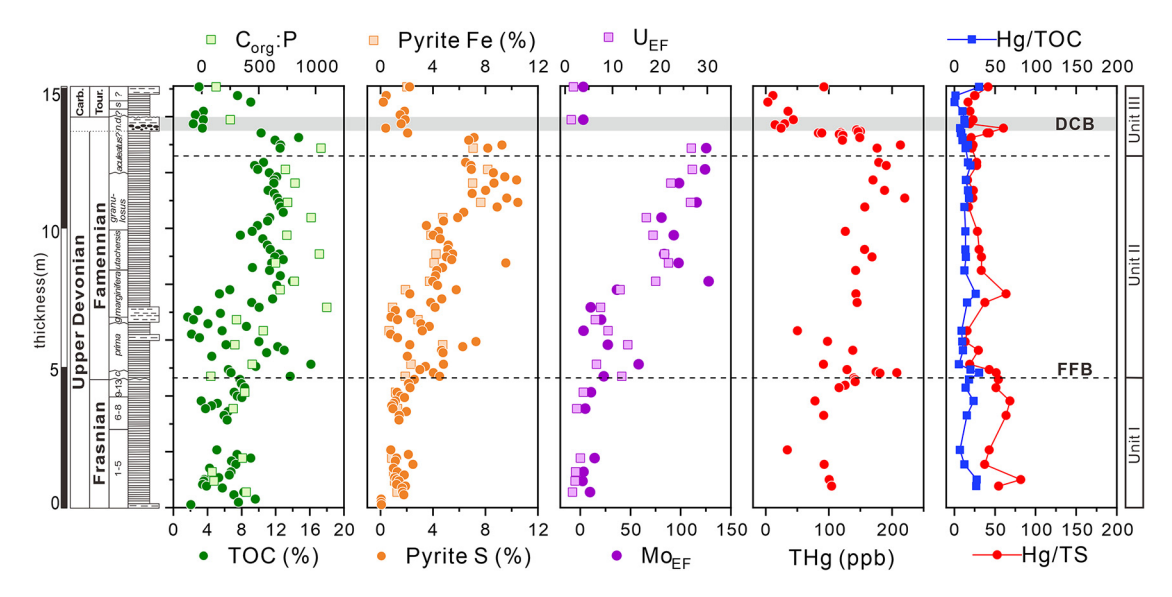


Fig. 2. Chemostratigraphy of total Hg (THg), common host phases of Hg in sediments (TOC, pyrite S, and pyrite Fe), Hg normalized to these host phases (Hg/TOC, Hg/TS), and published redox proxies (see details in Supplementary Text S3), including trace element enrichment factors (Mo_{EF}, U_{EF}), pyrite content, and C_{org}/P molar ratio. The two horizontal dashed lines separate Unit I (0-4.7 m), Unit II (4.7-12.6 m), and Unit III (12.6-15 m). The horizontal gray band marks the DCB interval. The data of TOC, TS, and redox proxies are from Song et al. (2021).

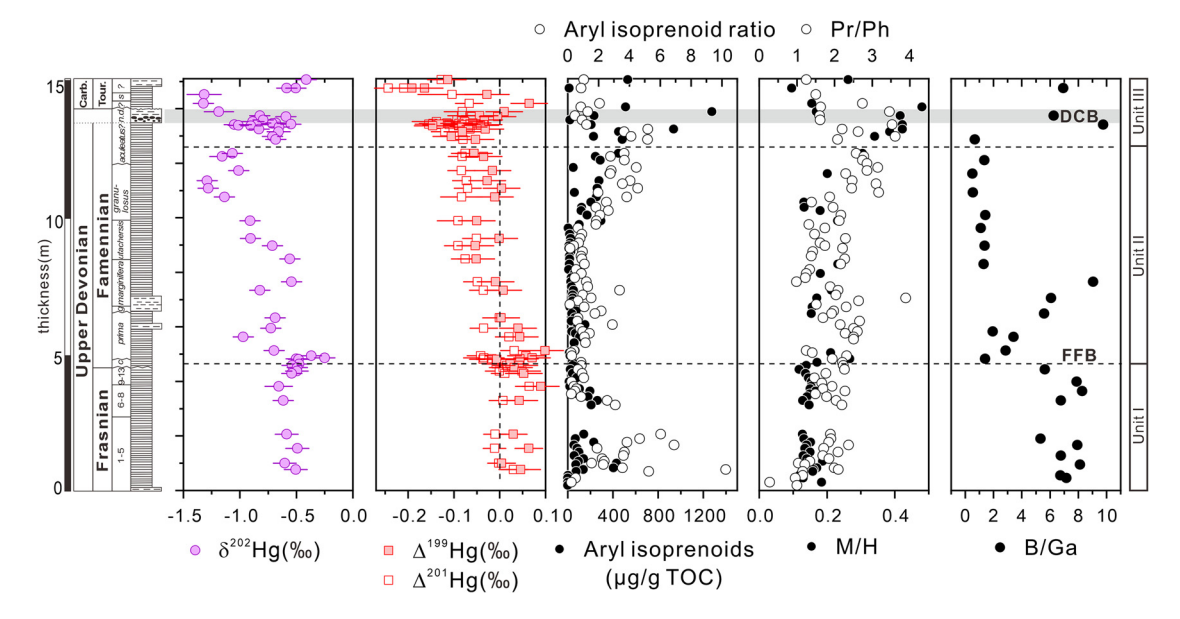


Fig. 3. Chemostratigraphy of Hg isotope compositions (δ^{202} Hg, Δ^{199} Hg, and Δ^{201} Hg), biomarkers that indicate PZE (aryl isoprenoids and aryl isoprenoid ratio) and terrestrial organic matter (pristane/phytane ratio [Pr/Ph] and moretane/hopane ratio [M/H]), and a salinity proxy (B/Ga). The two horizontal dashed lines and the horizontal gray band are defined the same as in Fig. 1. The biomarker and B/Ga data are from Song et al. (2021).

m); Unit II (4.7 to 12.6 m) contains most of the Famennian Stage; and Unit III (12.6 to 15 m) encompasses the uppermost Famennian to lowermost Mississippian, spanning the DCB (Over et al., 2019; Song et al., 2021) (Fig. 2). These units show significantly different values and patterns of secular variation in total Hg concentrations (THg), Hg isotopes, and other geochemical proxies (i.e., biomarker, and elemental redox and salinity proxies) (Figs. 2 and 3). Unit I shows a relatively small variation of THg (106 \pm 65 ppb, 2SD), nearly invariant δ^{202} Hg (representing MDF, $-0.55 \pm 0.12\%$, 2SD), and zero to slightly positive odd-MIF values (Δ^{199} Hg and Δ^{201} Hg, $0.01 \pm 0.04\%$ and $0.05 \pm 0.04\%$, respectively). Unit II shows a progressive increase in THg and simultaneous negative shifts of both δ^{202} Hg (down to -1.29%) and odd-MIF (down to -0.08%) for Δ^{201} Hg). Unit III is marked by a rapid decline in THg from 213 ppb to a minimum of 3.8 ppb at the top of the core. The Hg isotopic compositions in Unit III show two prominent negative excursions of odd-MIF with correlated positive excursions of $\delta^{202} \rm Hg.$ The first negative excursion of odd-MIF (down to -0.13% and -0.15% for $\Delta^{199} \rm Hg$ and $\Delta^{201} \rm Hg$, respectively) occurs slightly below the DCB interval, followed by an even stronger negative shift to -0.19% and -0.24% (for $\Delta^{199} \rm Hg$ and $\Delta^{201} \rm Hg$, respectively) within the Lower Mississippian. A less prominent negative excursion of odd-MIF is also observed just above the FFB in Unit II. The three negative excursions of odd-MIF were all accompanied by concurrent positive excursions of $\delta^{202} \rm Hg$. THg was also normalized to major host phases of Hg, i.e., organic matter (as proxied by total organic carbon, TOC) and sulfide minerals (as proxied by total sulfur, TS), and the normalized ratios (Hg/TOC and Hg/TS) show no significant peaks or discernible trends.

In previous studies, the Hg odd-MIF (Δ^{199} Hg and Δ^{201} Hg) was typically reported using the Δ^{199} Hg value alone (Blum and Bergquist, 2007; Blum et al., 2014). In our study, while Δ^{199} Hg and

 $\Delta^{201} \rm Hg$ show similar trends and yield a $\Delta^{199} \rm Hg/\Delta^{201} \rm Hg$ slope (m) of ~ 1.00 for all samples (Fig. S1), $\Delta^{201} \rm Hg$ is slightly more negative than $\Delta^{199} \rm Hg$ (Fig. 3). This led to smaller $\Delta^{199} \rm Hg$ than $\Delta^{201} \rm Hg$ values, particularly in Units II and III, where negative shifts of odd-MIF are observed. Thus, reporting odd-MIF using $\Delta^{199} \rm Hg$ alone may impede correct interpretation of odd-MIF variation. However, in order to facilitate comparisons with previous studies, $\Delta^{199} \rm Hg$ is still chosen to represent odd-MIF, but $\Delta^{201} \rm Hg$ is also reported when deemed useful. The even-MIF values ($\Delta^{200} \rm Hg$ and $\Delta^{204} \rm Hg)$ are indistinguishable from analytical error for all samples (Table S2). Therefore, we do not discuss even-MIF, and "MIF" refers only to odd-MIF in the following discussion.

5. Discussion

5.1. The indigeneity and syngeneity of Hg MDF and MIF

The THg and Hg isotopic compositions of the study samples are unlikely to have been altered by post-depositional diagenetic or metamorphic processes because the Dupont core was never deeply buried and experienced maximum burial temperatures of only 50-120 °C (Song et al., 2021), resulting in good preservation of its biomarker components (see Supplementary Text S2). Also unlikely is post-depositional gain of Hg in the study core, which consists of laminated black shale without evidence of bioturbation or signs of authigenic or diagenetic additions other than pyrite (Over et al., 2019). Therefore, both the MIF and MDF values are likely to represent indigenous primary signals. Since variations of MIF and MDF are tightly correlated throughout the study core (see details in Sections 5.4 and 5.5), we interpret δ^{202} Hg and Δ^{199} Hg values jointly in the discussion below. The coupled use of δ^{202} Hg and Δ^{199} Hg is subject to the caveat that MDF is thought to be more susceptible to fractionation processes in seawater and sediments than MIF. However, the relationship between MDF and MIF has been widely applied as a useful approach in modern environments to distinguish between different Hg sources and processes (Blum et al., 2014; Jiskra et al., 2021). The variation of δ^{202} Hg in sedimentary rocks should not be disregarded simply because it has potential complexities, and it can actually help to resolve mechanisms of MIF variation by providing an additional "dimension" to isotopic interpretations. While dedicated studies are still needed to better constrain the potential influences of various Hg sources and processes on δ^{202} Hg in the ocean, the most straightforward explanation for the covariation between δ^{202} Hg and Δ^{199} Hg in the current study is that they were driven by common sources or shared processes. In the following discussion, we will take advantage of the full strength of Hg isotopes by considering all patterns of Hg isotope variation, including the direction and magnitude of odd-MIF as well as the relationship between odd-MIF and MDF.

5.2. Lack of Hg enrichment provides no evidence for LIPs

Anomalous Hg enrichments across the FFB have been reported for a number of localities in Laurussia and South China that are geographically widely separated, and a link to an imprecisely dated LIP (i.e., the Viluy Traps of Siberia) has been proposed (Racki et al., 2018; Racki, 2020; Kaiho et al., 2021). Hg anomalies across the DCB have also been reported for sections in South China and Europe (Paschall et al., 2019; Kalvoda et al., 2019; Rakociński et al., 2020; Racki, 2020; Kaiho et al., 2021). These putative Hg anomalies led to the proposal that LIP magmatism was the major trigger of Late Devonian environmental and biotic crises (Racki, 2020).

However, not all Upper Devonian localities show Hg anomalies. Two recent publications reported no Hg enrichment at the FFB in multiple Upper Devonian sections from the Appalachian and Illinois basins (Liu et al., 2021) and South China (Zhao et al., 2022).

The present study section also did not yield any significant peaks in either raw or normalized Hg concentrations at the FFB or DCB, or at any other level in the core (Fig. 2). It is possible that Hgenriched boundary intervals are missing due to disconformities in the Dupont core, as the first Famennian conodont zone recognized in the study core is *crepida* which rests directly on condensed strata of Frasnian conodont zones (FZ) 12-13, indicating a hiatus across the FFB (Over et al., 2019). Despite this disconformity, published redox proxies (Corg/P, wt.% pyrite S, wt.% pyrite Fe, Mo_{EF}, U_{EF}) show continuous variation through the FFB interval (Supplementary Text S3). The depth profile of THg is almost identical to those of these proxies, and THg shows a good linear correlation with both TOC and TS throughout the entire study section (Fig. S2), suggesting a first-order control on Hg accumulation by oceanic redox conditions.

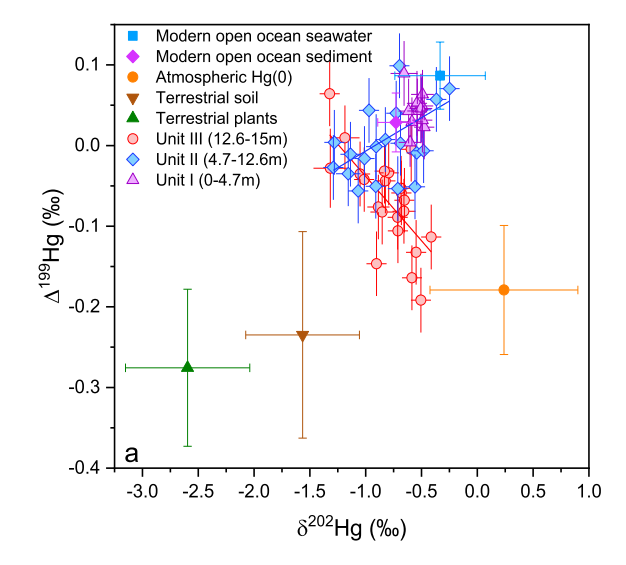
The complete lack of Hg anomalies in the entire study core which covers most of the Upper Devonian argues against largescale LIP activity in the Late Devonian. The presence of Hg anomalies in some but not all Late Devonian sections studied globally may be explained by the fact that Hg enrichment in sedimentary rocks is not always due to LIPs, but can also be caused by other types of Hg fluxes (such as submarine hydrothermal vent, arc volcanism, terrestrial soil erosion, and wildfire) (Them et al., 2019) or oceanic anoxia/euxinia-related processes (Zheng et al., 2018; Shen et al., 2019). It has also been suggested that the presence of Hg enrichment in some but not all localities reflects local volcanism rather than global LIPs (Zhao et al., 2022). Although potential candidates for a contemporaneous LIP during the FFB event (e.g., the Viluy Traps) have been identified, not all LIPs are capable of perturbing the global Hg cycle (Percival et al., 2018b). Therefore, the absence of widespread Hg anomalies in the Upper Devonian of both North America and South China suggests that LIPs were either absent or of limited size and impact during the two major extinction episodes, which argues against the hypothesis that the Late Devonian mass extinctions were triggered by LIP activity. This argument is further supported by our Hg isotope dataset, as discussed below.

5.3. Hg isotope baseline in the Chattanooga Shale (Unit I)

The Hg isotope compositions of Unit I (zero to slightly positive $\Delta^{199}{\rm Hg}$ and $\Delta^{201}{\rm Hg}$, negative $\delta^{202}{\rm Hg})$ are similar to those of modern open-ocean seawater and pre-anthropogenic sediments (Gehrke et al., 2009; Blum et al., 2014; Jiskra et al., 2021) (Fig. 4). The Hg isotope compositions of modern marine sediments typically reflect mixing between atmospheric and terrestrial inputs of Hg (Thibodeau and Bergquist, 2017; Grasby et al., 2019), which have markedly different isotopic signatures (Fig. S3 and Supplementary Text S4). The open-ocean sediments are typically dominated by atmospheric Hg inputs (Gehrke et al., 2009; Blum et al., 2014). Thus, the similar Hg isotope compositions of Unit I as the modern open-ocean sediments, together with the relatively low THg of the former, suggest that Unit I was dominated by the background atmospheric Hg deposition. Therefore, Unit I can be considered as a "baseline" signal for Hg isotopes in the Chattanooga Shale.

5.4. Hg isotope evidence for increasing terrestrial inputs in the Late Devonian

The concurrent negative shifts of δ^{202} Hg and Δ^{199} Hg in Unit II suggest a progressive increase of terrestrial Hg inputs due to enhanced erosion of terrestrial OM (note that the lowermost Unit II, in which δ^{202} Hg and Δ^{199} Hg shift in opposite directions, is an exception linked to PZE; see Section 5.5). Among the major sources of Hg to the ocean, only terrestrial Hg exhibits both negative MIF



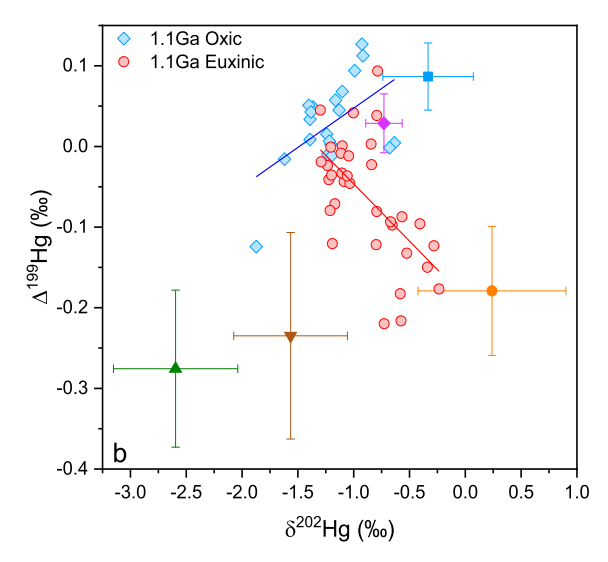


Fig. 4. Crossplots of $\Delta^{199} \rm Hg$ vs. $\delta^{202} \rm Hg$ for the a) Chattanooga Shale (this study) and b) 1.1 Ga Atar and El Mreiti Group (Zheng et al., 2018). The averages of literature data for modern terrestrial soil and plants, atmospheric Hg(0), and open ocean seawater and sediments are also plotted to demonstrate the isotope compositions of possible Hg sources. Please refer to supplementary Fig. S3 and Text S4 for a complete description and references for these literature data. In panel (a), the blue and red lines are linear regressions for Unit I + II (slope = 0.08 \pm 0.02, 1SE, $R^2 = 0.29$, P < 0.01) and Unit III (slope = -0.16 ± 0.04 , 1SE, $R^2 = 0.44$, P < 0.001), respectively. In panel (b), the blue and red lines are linear regressions for sediments deposited under oxic (slope = 0.10 ± 0.04 , 1SE, $R^2 = 0.27$, P < 0.02) and PZE conditions (slope = -0.16 ± 0.04 , 1SE, $R^2 = 0.44$, P < 0.001), respectively. The error bar for the literature data is 1SD. The error bar for samples in this study is the analytical error, as defined in the methods section.

and MDF values (Fig. S3 and Text S4). This means marine sediments with a larger terrestrial Hg fraction tend to develop concurrent negative MIF and MDF shifts relative to sediments dominated by background atmospheric Hg deposition, which tends to have slightly positive MIF and less negative MDF values (Blum et al., 2014; Grasby et al., 2017; Thibodeau and Bergquist, 2017; Kwon et al., 2020). Moreover, modern terrestrial samples have a characteristic positive relationship between $\Delta^{199} \rm Hg$ and $\delta^{202} \rm Hg$ $(m=0.13, R^2=0.78, P<0.01, Fig. S3)$ (Kwon et al., 2020), which is similar to the $\Delta^{199} \rm Hg/\delta^{202} \rm Hg$ relationship for Units I and II $(m=0.08\pm0.02, 1\rm SE, R^2=0.29, P<0.01)$ (Fig. 4). Because Unit I represents the "baseline" in which atmospheric deposition is the dominant Hg source, the concurrent negative shifts of $\delta^{202} \rm Hg$ and $\Delta^{199} \rm Hg$ in Unit II, as well as the similarity of its $\Delta^{199} \rm Hg/\delta^{202} \rm Hg$ to that of

modern terrestrial Hg, are consistent with a scenario of progressively increasing terrestrial Hg inputs during the accumulation of Unit II.

Increased terrestrial inputs to the interior basins of eastern North America during the Famennian are further supported by published biomarker proxies for terrestrial OM (Fig. 3), including moretane/hopane (M/H) and pristane/phytane (Pr/Ph) ratios (Song et al., 2021; Liu et al., 2021). Both ratios show consistent increases upward within Unit II. High M/H ratios have been observed in sediments with greater inputs from terrestrial soil erosion (Xie et al., 2007). Pr/Ph in the present study section was also interpreted to represent terrestrial OM inputs because one of the most common sources of pristane and phytane in marine sediments is terrestrial plant debris (Song et al., 2021). Thus, the simultaneous increases of Pr/Ph and M/H suggest enhanced terrestrial OM inputs to Unit II, supporting our Hg isotope interpretations. There is also abundant evidence for increased terrestrial runoff and soil erosion during the Late Devonian from various other organic and inorganic proxies (Algeo et al., 1995; Marynowski et al., 2012; Kaiho et al., 2013; Percival et al., 2019; Smart et al., 2022).

Increased terrestrial OM inputs to Unit II may have been linked to the expansion of land plants. The expansion of terrestrial floras due to the development of trees and seed plants with deep root systems in the Late Devonian presumably enhanced soil formation and weathering, and increased runoff and riverine fluxes of Hg associated with terrestrial OM (Algeo et al., 1995; Algeo and Scheckler, 1998; Liu et al., 2019; Zhang et al., 2020). It remains an open question whether the spread of land plants was a gradual process accounting only for long-term trends in the Devonian (such as declining atmospheric pCO₂) or a punctuated process that triggered short-term events such as the FFB and DCB. Although the temporal resolution of Devonian paleobotanic records is generally insufficient to address this issue, it is relevant that modern invasive floral species can spread at rates of kilometers per year (Horvitz et al., 2017), permitting complete colonization of continents at geologically instantaneous timescales. Moreover, the Late Pleistocene-Holocene climate change triggered rapid vegetational shifts (Williams et al., 2009). These examples provide analogs for the tempo and consequences of the spread of Devonian land plants into new continental realms.

Changes in global sea level during the Late Devonian may have also contributed to widespread erosion of exposed continental shelves and basin margins, thus increasing terrestrial OM and Hg inputs to marine systems. Following a lowstand at the FFB, eustatic levels rose during the early to mid-Famennian (Johnson et al., 1985; Sandberg et al., 2002) but subsequently began to fall by the aculeatus Zone (Algeo et al., 2007; Algeo and Maynard, 2008; Song et al., 2021). However, the paleosalinity proxy (B/Ga ratio) indicates that the watermass salinity within the Illinois Basin shifted from (near-)marine conditions in the Frasnian to low-brackish conditions in the Famennian (Song et al., 2021) (Fig. 3), despite a concurrent rise in sea level. This pattern suggests major changes in watershed hydrology. Specifically, low B/Ga values on the basin's outer margin (i.e., Cumberland Sill) are an indication of a greatly expanded low-salinity surface layer, linked to increased runoff within the basin's watershed that may have been triggered by enhanced evapotranspiration as a consequence of expanding terrestrial floral biomass (Algeo et al., 1995; Algeo and Scheckler, 1998).

Enhanced terrestrial erosion can also account for the euxinic bottom-water conditions and tightly correlated increases of THg and redox proxies recorded in Unit II (Fig. 2). Terrestrial weathering and erosion deliver vital nutrients and trace metals to the ocean, which can stimulate marine primary productivity and thus increase the consumption of dissolved oxygen through remineralization of both marine and terrestrial OM. This process is well

supported as a plausible cause of widespread anoxia in the Late Devonian oceans (Algeo et al., 1995, 2007; Liu et al., 2019; Percival et al., 2020; Zhang et al., 2020). Terrestrial erosion may also deliver sulfate to the ocean, which can promote euxinia through microbial sulfate reduction. Thus the tight correlation between Hg and various redox proxies (Fig. 2) is likely due to enhanced scavenging of Hg by OM and sulfide from the water column, which is evidenced by the positive relationships of THg with both TOC ($R^2 = 0.32$) and TS ($R^2 = 0.63$) (Fig. S2).

5.5. Hg isotope evidence for recurrent PZE across the FFB and DCB

The high-resolution Hg isotope dataset of the study core reveals at least three episodes of distinct negative excursions of Hg MIF alongside concurrent positive excursions of MDF, with the two most prominent excursions in Unit III (just below and above DCB) and another one in the lowermost Unit II (just above FFB) (Fig. 3). These distinct excursions of Hg isotopes cannot be explained by either volcanic or enhanced terrestrial inputs, because they are not associated with any anomalous Hg enrichment (see Section 5.2), and the relationships between MIF and MDF for the three excursions are opposite to those observed for modern terrestrial Hg as well as Unit II of the present study core, for which a gradual increase of terrestrial Hg inputs is plausible (see Section 5.4). Modern terrestrial Hg and Unit II both show a positive relationship between Δ^{199} Hg and δ^{202} Hg (Figs. 4 and S3). In contrast, Unit III, which contains two prominent excursions, shows a negative correlation between Δ^{199} Hg and δ^{202} Hg with a slope of -0.16 $(R^2 = 0.44, P < 0.001)$ (Fig. 4a).

We propose that the three negative excursions of $\Delta^{199} Hg$ alongside positive excursions of δ^{202} Hg reflect three episodes of PZE. This hypothesis is consistent with previous findings that PZE was a widespread and frequent recurring marine condition in the Late Devonian, and there is abundant evidence for PZE at both the FFB and DCB on the Laurentian Craton (Liu et al., 2019; Kabanov and Jiang, 2020). A main piece of evidence for our hypothesis is that, at least two of these excursions of Hg isotopes (the two in Unit III) coincided with increases of biomarkers for PZE, i.e., aryl isoprenoids (AI) and the short-chain (C₁₃-C₁₇) to intermediatechain (C₁₈-C₂₂) AI ratio (AIR) (see Supplementary Text S3 for details of biomarkers). Although the excursion just above the FFB is not associated with any apparent increase of these biomarkers (Fig. 3), it should be noted that our Hg isotope profile was generated from a set of samples with a much higher resolution across the FFB (i.e., double the sample density) than that measured for biomarkers. It has been shown that the PZE condition at the FFB was transient and fluctuating in the Appalachian Basin (Haddad et al., 2018), and thus it may have been only recorded by the higherresolution Hg isotope profile.

Another important reason to link the three Hg isotope excursions to PZE is that both the magnitude and direction of Hg isotope excursions of the current study are very similar to those observed in Mesoproterozoic (1.1 Ga) black shales from the Atar and El Mreiti Group, West Africa (Zheng et al., 2018). The Mesoproterozoic study found that sediments deposited under PZE (identified by biomarker data) tend to develop significantly more negative MIF values (by as much as $\sim -0.2\%$) than those deposited under oxic water columns. In the present study, the peak odd-MIF values of the two more prominent negative excursions in Unit III (-0.19% and -0.13% for Δ^{199} Hg, and -0.24% and -0.15% for Δ^{201} Hg, Table S2) are similar in magnitude to the negative excursion reported for Mesoproterozoic shales deposited under PZE. More importantly, the relationship and slopes between Δ^{199} Hg and δ^{202} Hg in the Chattanooga Shale are surprisingly similar to those of Mesoproterozoic black shales (Zheng et al., 2018), which also show a positive correlation for sediments deposited in an oxic

water column (m=0.10, P < 0.02) and a negative correlation for sediments deposited under PZE (m=-0.16, P < 0.001) (Fig. 4b). Note that the Mesoproterozoic terrestrial environment likely had a much smaller Hg reservoir and different Hg isotopic signature than those during the Late Devonian because a major terrestrial Hg reservoir, plants and topsoil, was absent during the Mesoproterozoic (Kenrick et al., 2012), yet these two time periods still show surprisingly similar patterns of Hg isotopes, consistent with our inference that terrestrial inputs cannot completely account for Hg isotope variation in Unit III.

The cause of Hg isotope fractionation during PZE is still under investigation, but two mechanisms are considered likely (Zheng et al., 2018): 1) photoreduction of Hg(II) complexed by reduced sulfur in a sulfide-rich photic zone, and 2) enhanced sequestration of atmospheric Hg(0) by sulfidic surface water (Fig. 5). Sulfidic water is found to enhance aqueous Hg(0) oxidation (Zheng et al., 2019), and, thus, the presence of PZE could facilitate uptake and sequestration of atmospheric Hg(0) by the oceans. The oxidation of atmospheric Hg(0) by sulfidic seawater produces negative MIF and positive MDF in Hg(II) with a Δ^{199} Hg/ δ^{202} Hg slope of ~ -0.12 (Zheng et al., 2019), which is similar to the slope observed for sediments deposited under PZE in the Upper Devonian Chattanooga Shale and Mesoproterozoic Atar/El Mreiti Group shales. Modern atmospheric Hg(0) itself has negative MIF and positive MDF with a Δ^{199} Hg/ δ^{202} Hg slope of -0.09 (Fig. S3). Thus, enhanced aqueous oxidation of atmospheric Hg(0) in sulfidic ocean-surface waters may have been responsible for the negative correlation between Hg MIF and MDF in these PZE settings. Moreover, photoreduction of Hg(II) in sulfidic water also produces negative MIF and positive MDF in the residual Hg(II) (Zheng and Hintelmann, 2010). Although the Δ^{199} Hg/ δ^{202} Hg obtained in photochemical experiments is much larger (~ -0.7) than those of the Chattanooga and Atar/El Mreiti shales, the $\Delta^{199} {\rm Hg}/\delta^{202} {\rm Hg}$ slope is dependent on experimental conditions, and the $\Delta^{199} {\rm Hg}/\Delta^{201} {\rm Hg}$ slope of all samples in the present study (\sim 1.0, Fig. S1) is consistent with photoreduction. Thus, it is possible that photoreduction also played a role in driving the covariation of δ^{202} Hg and odd-MIF under PZE settings.

6. Implications for Late Devonian biocrises

6.1. PZE linked to enhanced terrestrial nutrient inputs

Biomarker records of PZE are present in Upper Devonian-Lower Mississippian strata of epicontinental basins throughout Laurussia including the Illinois Basin, in which the present study section is located (see summary in Kabanov and Jiang, 2020). Such widespread PZE was likely driven by a mechanism operating at a continental or global scale. LIPs have been widely invoked as a trigger of oceanic anoxia during mass extinctions. However, we have already argued based on the lack of Hg enrichment that the impact of LIPs was likely quite limited during both the FFB and DCB events (see Section 5.2). Furthermore, LIPs typically result in positive shifts of Hg MIF due to photochemical redox reactions of Hg during atmospheric transport (Thibodeau and Bergquist, 2017; Grasby et al., 2019), which is clearly opposite to the negative excursions of Hg MIF across both extinction horizons in our study section

We hypothesize that the widespread and recurrent PZE in the Late Devonian was linked to increased terrestrial nutrient inputs to marine systems as a consequence of the expansion of terrestrial plants and/or changes of global sea level (Algeo et al., 1995; Algeo and Scheckler, 1998) (Fig. 5). The variation of Hg isotopes in Unit II has already shown evidence of a long-term, progressive increase of terrestrial inputs (see Section 5.4). Although a direct causal link between enhanced terrestrial inputs and PZE is difficult to confirm with Hg isotopes alone, additional evidence is that

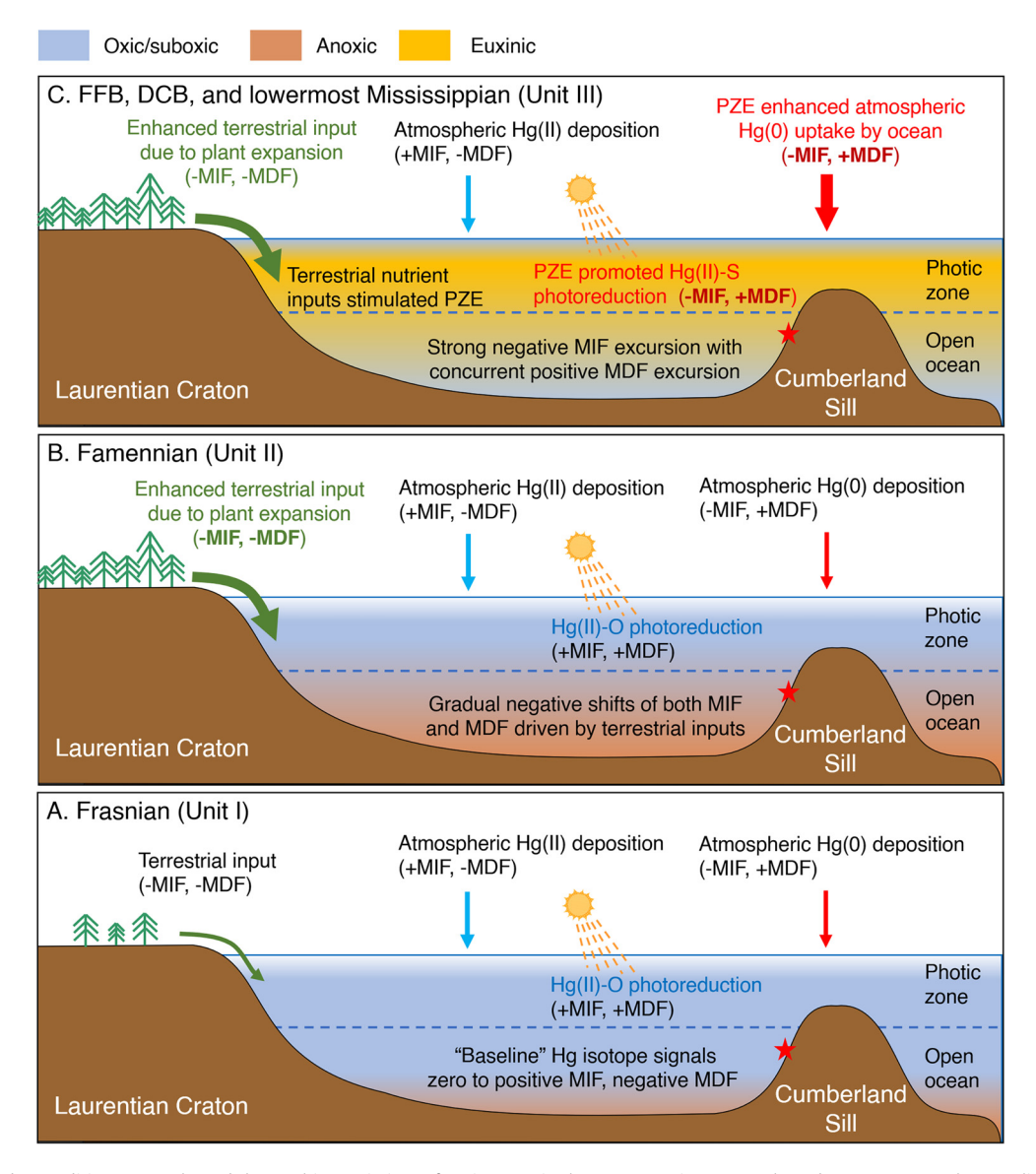


Fig. 5. Evolution of redox conditions, Hg cycle, and the resulting variations of Hg isotopes in the Late Devonian ocean. The red star represents the sampling location. "Hg(II)-O" denotes Hg(II) complexed by oxygen functional groups in organic matter (e.g., carboxyl) and "Hg(II)-S" denotes Hg(II) complexed by reduced sulfur groups.

abundant phosphate nodules were found in the gray shale strata of the DCB interval in the Chattanooga Shale, as well as on the southern continental margin of Laurussia (Over, 2020). In fact, sedimentary phosphate enrichments are widely found in black shales of the Upper Kellwasser (just above FFB) and Hangenberg events (just below DCB) in multiple locations around Laurussia (Percival et al., 2020) and the South China Craton (Paschall et al., 2019), consistent with an enhanced nutrient influx as the initial trigger of oceanic anoxia during the Late Devonian (Algeo et al., 1995; Algeo and Scheckler, 1998; Murphy et al., 2000). Elevated marine productivity and PZE driven by terrestrially sourced nutrients have been documented in conjunction with various major events in Earth history. For example, widespread PZE was also recorded in continental margins at the end-Permian mass extinction (Grice, 2005), and was thought to have been driven by enhanced terrestrial nutrient inputs (Schobben et al., 2020) and upper ocean nutrient (phosphate) recycling (Hülse et al., 2021). The accumulation of P in sediments typically requires oxic or ferruginous conditions, whereas euxinic conditions would redissolve and recycle P in sediments back to the water column (Murphy et al., 2000; Canfield et al., 2020). This process of P cycling is proposed to have been a key mechanism driving ocean productivity and triggering anoxia during the Late

Devonian and other mass extinction events (Percival et al., 2020; Schobben et al., 2020). The fluctuating redox conditions of Unit III in the study core (Supplementary Text S3) would have facilitated preservation of P during non-euxinic intervals and its release and recycling during euxinic intervals. Thus, the occurrence of phosphate-rich layers in Unit III and the widespread P enrichment in Laurussia epicontinental settings around both the FFB and DCB coincide with episodes of PZE identified by Hg isotopes, suggesting that enhanced P influx and recycling in the water column may have contributed to the development of PZE.

The expansion of rooted vascular plants was probably the most critical bioevolutionary development of the Late Devonian (Algeo et al., 1995; Algeo and Scheckler, 1998) and is thought to have triggered contemporaneous major environmental changes, including enhanced terrestrial weathering and global cooling as a consequence of atmospheric CO₂ removal (Berner, 1997), which in turn led to a global sea-level fall via formation of glaciers and continental icesheets (Brezinski et al., 2008). This global sea-level fall began in the late Famennian (*aculeatus* Zone) and reached a lowstand at the DCB (Johnson et al., 1985; Sandberg et al., 2002; Algeo et al., 2007; Algeo and Maynard, 2008), despite interruption by a major transgression associated with deposition of the Hangen-

berg Black Shale (Sahoo et al., 2023). The global sea-level fall would have exposed continental shelves and basin margins, thus enhancing terrestrial weathering, and increased watermass restriction within some epicontinental basins, promoting development of PZE through intensified water-column stratification.

6.2. Relationship between PZE and mass extinctions

The Late Devonian was characterized by multiple biotic crises including the Lower and Upper Kellwasser crises near the FFB, and the Annulata, Dasberg, and Hangenberg crises near the DCB (Walliser, 1996). The FFB marks the largest extinction event of the Late Devonian, and our Hg isotope dataset indeed shows evidence of PZE just above the FFB. However, the excursions of Hg isotopes in the lowermost Famennian are quite transient and roughly correspond to the crepida conodont Zone, post-dating the Kellwasser crises (Carmichael et al., 2019). Thus, we are unable to directly link PZE to the extinction at the FFB. The Hangenberg Crisis, which immediately preceded the DCB, represents the second largest and final pulse of the Late Devonian mass extinction. Marine invertebrate taxa were severely affected, particularly shallow-water reef communities that had already suffered declines during the Kellwasser Events (Kaiser et al., 2016). However, due to the lack of conodont zones that represent the Hangenberg Event in the Chattanooga Shale, we cannot precisely link PZE to the Hangenberg Crisis.

Despite the above limitations, our study of the Chattanooga Shale reveals that PZE started to develop prior to the DCB lowstand, and that it may have persisted across the DCB and into the earliest Mississippian, thus supporting PZE as a potential kill mechanism for shallow-water taxa during the Devonian-Carboniferous transition, at least in the Illinois Basin. The onset of PZE corresponds to the Dasberg Event based on the available conodont biostratigraphic data (Over et al., 2019; Over, 2020). The Dasberg Event is recognized globally by organic-rich black shales deposited during a eustatic rise, with biomarker evidence for PZE (Marynowski et al., 2010, 2012). The Dasberg Crisis involved significant faunal turnover and reorganization among marine invertebrates such as ammonoids, rugose coral, and brachiopods (particularly well-documented in Europe) (Marynowski et al., 2010), as well as the development of a sponge-microbe symbiont "disaster bed" in shallow-marine strata of western North America, indicative of extinction of diverse, neritic taxa (Stock and Sandberg, 2019). Furthermore, shallow-water euxinia immediately prior to the DCB lowstand has also been documented in other epicratonic seas across North America including in the Cleveland Shale of the Appalachian Basin (Martinez et al., 2019) and the Bakken Shale of the Williston Basin (Sahoo et al., 2023), supporting the widespread and recurrent nature of PZE across the Devonian-Carboniferous transition. Together, inorganic and organic geochemical data from multiple sections worldwide, including novel Hg isotope results from this study, support recurrent PZE as a possible kill mechanism for the Late Devonian mass extinctions, although more studies are needed to verify this hypothesis.

7. Conclusions

Our high-resolution Hg isotope dataset, together with published biomarker proxy data, makes a strong case for recurrent PZE in the epicontinental seas of North America during the Late Devonian, which may have been a key kill mechanism for the contemporaneous mass extinctions. Notably, Hg isotopes also reveal that the PZE interval was preceded by a long-term, progressive increase of terrestrial inputs of OM and nutrients during the Famennian, which may have stimulated marine primary productivity and eventually

contributed to the development of widespread PZE. Also importantly, the PZE around both the FFB and DCB and the enhanced terrestrial weathering during the Famennian were not triggered by global-scale volcanism, as evidenced by the lack of Hg enrichments during either the FFB or DCB events in the present study section as well as in other Upper Devonian sections of eastern North America. Thus, our findings do not support an LIP as the trigger of the environmental and biotic crises of the Late Devonian. Lastly, our results also demonstrate the potential of Hg isotopes as a novel proxy for both PZE and terrestrial OM erosion, providing new insights into the mechanism and impact of ocean-redox changes on Earth's habitability. This is not only important for reconstructing the evolution of life in the geological past, but also critical for predicting future biotic crises related to global-warming-induced expansion of anoxic "dead zones" in the modern ocean.

CRediT authorship contribution statement

Wang Zheng: Conceptualization, Investigation, Methodology, Supervision, Writing – original draft. Geoffrey J. Gilleaudeau: Conceptualization, Resources, Writing – review & editing. Thomas J. Algeo: Resources, Visualization, Writing – review & editing. Yaqiu Zhao: Investigation. Yi Song: Resources, Visualization, Writing – review & editing. Yuanming Zhang: Investigation. Swapan K. Sahoo: Validation, Writing – review & editing. Ariel D. Anbar: Validation, Writing – review & editing. Sarah K. Carmichael: Validation, Writing – review & editing. Shucheng Xie: Validation, Writing – review & editing. Cong-Qiang Liu: Validation, Writing – review & editing. Jiubin Chen: Funding acquisition, Supervision.

Declaration of competing interest

The authors declare that they have no known competing financial interests or personal relationships that could have appeared to influence the work reported in this paper.

Data availability

The datasets used in this study will be made publicly available in the supplementary material.

Acknowledgements

Funding: This work was financially supported by the National Natural Science Foundation of China (grant No. 41973009, 41625012) and National Science Foundation of United States (award No. EAR 1760203 to A.D.A.). G.J.G. thanks the NASA Post-doctoral Program, which provided funds for travel and sample collection. We thank Pengfei Li and Lixin Zhang for assistance with MC-ICP-MS measurements.

Appendix A. Supplementary material

Supplementary material related to this article can be found online at https://doi.org/10.1016/j.epsl.2023.118175.

References

Algeo, T.J., Berner, R.A., Maynard, J.B., Scheckler, S.E., 1995. Late Devonian oceanic anoxic events and biotic crises: "rooted" in the evolution of vascular land plants? GSA Today 24.

Algeo, T.J., Lyons, T.W., Blakey, R.C., Over, D.J., 2007. Hydrographic conditions of the Devono-Carboniferous North American Seaway inferred from sedimentary Mo-TOC relationships. Palaeogeogr. Palaeoclimatol. Palaeoecol. 256, 204–230.

Algeo, T.J., Maynard, J.B., 2008. Trace-metal covariation as a guide to water-mass conditions in ancient anoxic marine environments. Geosphere 4, 872.

- Algeo, T.J., Scheckler, S.E., 1998. Terrestrial-marine teleconnections in the Devonian: links between the evolution of land plants, weathering processes, and marine anoxic events. Philos. Trans. R. Soc. Lond. B, Biol. Sci. 353, 113–130.
- Averbuch, O., Tribovillard, N., Devleeschouwer, X., Riquier, L., Mistiaen, B., Van Vliet-Lanoe, B., 2005. Mountain building-enhanced continental weathering and organic carbon burial as major causes for climatic cooling at the Frasnian-Famennian boundary (c. 376 Ma)? Terra Nova 17, 25–34.
- Berner, R.A., 1997. The rise of plants and their effect on weathering and atmospheric CO2. Science 276, 544–546.
- Blum, J.D., Bergquist, B.A., 2007. Reporting of variations in the natural isotopic composition of mercury. Anal. Bioanal. Chem. 388, 353–359.
- Blum, J.D., Johnson, M.W., 2017. Recent developments in Mercury stable isotope analysis. Rev. Mineral. Geochem. 82, 733–757.
- Blum, J.D., Sherman, L.S., Johnson, M.W., 2014. Mercury isotopes in Earth and environmental sciences. Annu. Rev. Earth Planet. Sci. 42, 249–269.
- Bond, D.P.G., Grasby, S.E., 2017. On the causes of mass extinctions. Palaeogeogr. Palaeoclimatol. Palaeoecol. 478, 3–29.
- Brezinski, D.K., Cecil, C.B., Skema, V.W., Stamm, R., 2008. Late Devonian glacial deposits from the eastern United States signal an end of the mid-Paleozoic warm period. Palaeogeogr. Palaeoclimatol. Palaeoecol. 268, 143–151.
- Canfield, D.E., Bjerrum, C.J., Zhang, S., Wang, H., Wang, X., 2020. The modern phosphorus cycle informs interpretations of Mesoproterozoic Era phosphorus dynamics. Earth-Sci. Rev. 208, 103267.
- Caplan, M.L., Bustin, R.M., 1999. Devonian–Carboniferous Hangenberg mass extinction event, widespread organic-rich mudrock and anoxia: causes and consequences. Palaeogeogr. Palaeoclimatol. Palaeoecol. 148, 187–207.
- Carmichael, S.K., Waters, J.A., Königshof, P., Suttner, T.J., Kido, E., 2019. Paleogeography and paleoenvironments of the Late Devonian Kellwasser event: A review of its sedimentological and geochemical expression. Glob. Planet. Change 183, 102984
- Gehrke, G.E., Blum, J.D., Meyers, P.A., 2009. The geochemical behavior and isotopic composition of Hg in a mid-Pleistocene western Mediterranean sapropel. Geochim. Cosmochim. Acta 73, 1651–1665.
- Grasby, S.E., Shen, W., Yin, R., Gleason, J.D., Blum, J.D., Lepak, R.F., Hurley, J.P., Beauchamp, B., 2017. Isotopic signatures of Mercury contamination in latest Permian oceans. Geology 45, 55–58.
- Grasby, S.E., Them, T.R., Chen, Z., Yin, R., Ardakani, O.H., 2019. Mercury as a proxy for volcanic emissions in the geologic record. Earth-Sci. Rev. 196, 102880.
- Grice, K., 2005. Photic zone euxinia during the Permian-Triassic superanoxic event. Science 307, 706–709.
- Haddad, E.E., Boyer, D.L., Droser, M.L., Lee, B.K., Lyons, T.W., Love, G.D., 2018. Ichnofabrics and chemostratigraphy argue against persistent anoxia during the Upper Kellwasser Event in New York State. Palaeogeogr. Palaeoclimatol. Palaeoecol. 490, 178–190.
- Horvitz, N., Wang, R., Wan, F.-H., Nathan, R., 2017. Pervasive human-mediated large-scale invasion: analysis of spread patterns and their underlying mechanisms in 17 of China's worst invasive plants. J. Ecol. 105, 85–94.
- Hülse, D., Lau, K.V., van de Velde, S.J., Arndt, S., Meyer, K.M., Ridgwell, A., 2021. End-Permian marine extinction due to temperature-driven nutrient recycling and euxinia. Nat. Geosci., 1–6.
- Jiskra, M., Heimbürger-Boavida, L.-E., Desgranges, M.-M., Petrova, M.V., Dufour, A., Ferreira-Araujo, B., Masbou, J., Chmeleff, J., Thyssen, M., Point, D., Sonke, J.E., 2021. Mercury stable isotopes constrain atmospheric sources to the ocean. Nature 597, 678–682.
- Johnson, J.G., Klapper, G., Sandberg, C.A., 1985. Devonian eustatic fluctuations in Euramerica. GSA Bull. 96, 567–587.
- Kabanov, P., Jiang, C., 2020. Photic-zone euxinia and anoxic events in a Middle-Late Devonian shelfal sea of Panthalassan continental margin, NW Canada: changing paradigm of Devonian ocean and sea level fluctuations. Glob. Planet. Change 188, 103153.
- Kaiho, K., Miura, M., Tezuka, M., Hayashi, N., Jones, D.S., Oikawa, K., Casier, J.-G., Fu-jibayashi, M., Chen, Z.-Q., 2021. Coronene, mercury, and biomarker data support a link between extinction magnitude and volcanic intensity in the Late Devonian. Glob. Planet. Change 199, 103452.
- Kaiho, K., Yatsu, S., Oba, M., Gorjan, P., Casier, J.-G., Ikeda, M., 2013. A forest fire and soil erosion event during the Late Devonian mass extinction. Palaeogeogr. Palaeoclimatol. Palaeoecol. 392, 272–280.
- Kaiser, S.I., Aretz, M., Becker, R.T., 2016. The global Hangenberg Crisis (Devonian–Carboniferous transition): review of a first-order mass extinction. In: Becker, R.T., Königshof, P., Brett, C.E. (Eds.), Devonian Clim. Sea Level Evol. Events. Geological Society of London.
- Kalvoda, J., Kumpan, T., Qie, W., Frýda, J., Bábek, O., 2019. Mercury spikes at the Devonian-Carboniferous boundary in the eastern part of the Rhenohercynian Zone (central Europe) and in the South China Block. Palaeogeogr. Palaeoclimatol. Palaeoecol. 531. 109221.
- Kenrick, P., Wellman, C.H., Schneider, H., Edgecombe, G.D., 2012. A timeline for terrestrialization: consequences for the carbon cycle in the Palaeozoic. Philos. Trans. R. Soc. Lond. B, Biol. Sci. 367, 519–536.
- Kwon, S.Y., Blum, J.D., Yin, R., Tsui, M.T.-K., Yang, Y.H., Choi, J.W., 2020. Mercury stable isotopes for monitoring the effectiveness of the Minamata Convention on Mercury. Earth-Sci. Rev. 203. 103111.

- Liu, J., Luo, G., Lu, Z., Lu, W., Qie, W., Zhang, F., Wang, X., Xie, S., 2019. Intensified ocean deoxygenation during the end Devonian mass extinction. Geochem. Geophys. Geosyst. 20, 6187–6198.
- Liu, Z., Percival, L.M.E., Vandeputte, D., Selby, D., Claeys, P., Over, D.J., Gao, Y., 2021. Upper Devonian mercury record from North America and its implications for the Frasnian–Famennian mass extinction. Palaeogeogr. Palaeoclimatol. Palaeoecol. 576, 110502.
- Marshall, J.E.A., Lakin, J., Troth, I., Wallace-Johnson, S.M., 2020. UV-B radiation was the Devonian-Carboniferous boundary terrestrial extinction kill mechanism. Sci. Adv. 6. eaba0768.
- Martinez, A.M., Boyer, D.L., Droser, M.L., Barrie, C., Love, G.D., 2019. A stable and productive marine microbial community was sustained through the end-Devonian Hangenberg Crisis within the Cleveland Shale of the Appalachian Basin, United States. Geobiology 17, 27–42.
- Marynowski, L., Filipiak, P., Zatoń, M., 2010. Geochemical and palynological study of the Upper Famennian Dasberg event horizon from the Holy Cross Mountains (central Poland). Geol. Mag. 147, 527–550.
- Marynowski, L., Zatoń, M., Rakociński, M., Filipiak, P., Kurkiewicz, S., Pearce, T.J., 2012. Deciphering the upper Famennian Hangenberg Black Shale depositional environments based on multi-proxy record. Palaeogeogr. Palaeoclimatol. Palaeoecol. 346–347, 66–86.
- Murphy, A.E., Sageman, B.B., Hollander, D.J., Lyons, T.W., Brett, C.E., 2000. Black shale deposition and faunal overturn in the Devonian Appalachian Basin: clastic starvation, seasonal water-column mixing, and efficient biolimiting nutrient recycling. Paleoceanography 15, 280–291.
- Over, D.J., 2020. The Devonian-Carboniferous boundary in the United States. Palaeobiodivers. Palaeoenviron.
- Over, D.J., Hauf, E., Wallace, J., Chiarello, J., Over, J.-S., Gilleaudeau, G.J., Song, Y., Algeo, T.J., 2019. Conodont biostratigraphy and magnetic susceptibility of Upper Devonian Chattanooga Shale, eastern United States: evidence for episodic deposition and disconformities. Palaeogeogr. Palaeoclimatol. Palaeoecol. 524, 137–149.
- Paschall, O., Carmichael, S.K., Königshof, P., Waters, J.A., Ta, P.H., Komatsu, T., Dombrowski, A., 2019. The Devonian-Carboniferous boundary in Vietnam: Sustained ocean anoxia with a volcanic trigger for the Hangenberg Crisis? Glob. Planet. Change 175, 64–81.
- Percival, L.M.E., Bond, D.P.G., Rakociński, M., Marynowski, L., Hood, A.v.S., Adatte, T., Spangenberg, J.E., Föllmi, K.B., 2020. Phosphorus-cycle disturbances during the Late Devonian anoxic events. Glob. Planet. Change 184, 103070.
- Percival, L.M.E., Davies, J.H.F.L., Schaltegger, U., De Vleeschouwer, D., Da Silva, A.-C., Föllmi, K.B., 2018a. Precisely dating the Frasnian-Famennian boundary: implications for the cause of the Late Devonian mass extinction. Sci. Rep. 8, 9578.
- Percival, L.M.E., Jenkyns, H.C., Mather, T.A., Dickson, A.J., Batenburg, S.J., Ruhl, M., Hesselbo, S.P., Barclay, R., Jarvis, I., Robinson, S.A., Woelders, L., 2018b. Does large igneous province volcanism always perturb the mercury cycle? Comparing the records of Oceanic Anoxic Event 2 and the end-Cretaceous to other Mesozoic events. Am. J. Sci. 318, 799–860.
- Percival, L.M.E., Ruhl, M., Hesselbo, S.P., Jenkyns, H.C., Mather, T.A., Whiteside, J.H., 2017. Mercury evidence for pulsed volcanism during the end-Triassic mass extinction. Proc. Natl. Acad. Sci. 114, 7929–7934.
- Percival, L.M.E., Selby, D., Bond, D.P.G., Rakociński, M., Racki, G., Marynowski, L., Adatte, T., Spangenberg, J.E., Föllmi, K.B., 2019. Pulses of enhanced continental weathering associated with multiple late Devonian climate perturbations: evidence from osmium-isotope compositions. Palaeogeogr. Palaeoclimatol. Palaeoecol. 524, 240–249.
- Racki, G., 2020. A volcanic scenario for the Frasnian–Famennian major biotic crisis and other Late Devonian global changes: more answers than questions? Glob. Planet. Change 189, 103174.
- Racki, G., Rakociński, M., Marynowski, L., Wignall, P.B., 2018. Mercury enrichments and the Frasnian-Famennian biotic crisis: a volcanic trigger proved? Geology 46, 543–546
- Rakociński, M., Marynowski, L., Pisarzowska, A., Bełdowski, J., Siedlewicz, G., Zatoń, M., Perri, M.C., Spalletta, C., Schönlaub, H.P., 2020. Volcanic related methylmercury poisoning as the possible driver of the end-Devonian Mass Extinction. Sci. Rep. 10, 1–8.
- Sahoo, S.K., Gilleaudeau, G.J., Wilson, K., Hart, B., Barnes, B.D., Faison, T., Bowman, A.R., Larsen, T.E., Kaufman, A.J., 2023. Basin-scale reconstruction of euxinia and Late Devonian mass extinctions. Nature 615, 640–645.
- Sallan, L.C., Coates, M.I., 2010. End-Devonian extinction and a bottleneck in the early evolution of modern jawed vertebrates. Proc. Natl. Acad. Sci. 107, 10131–10135.
- Sandberg, C.A., Morrow, J.R., Ziegler, W., 2002. Late Devonian sea-level changes, catastrophic events, and mass extinctions.
- Schobben, M., Foster, W.J., Sleveland, A.R.N., Zuchuat, V., Svensen, H.H., Planke, S., Bond, D.P.G., Marcelis, F., Newton, R.J., Wignall, P.B., Poulton, S.W., 2020. A nutrient control on marine anoxia during the end-Permian mass extinction. Nat. Geosci. 13, 640–646.
- Shen, J., Algeo, T.J., Chen, J., Planavsky, N.J., Feng, Q., Yu, J., Liu, J., 2019. Mercury in marine Ordovician/Silurian boundary sections of South China is sulfide-hosted and non-volcanic in origin. Earth Planet. Sci. Lett. 511, 130–140.

- Shi, M., Bergquist, B.A., Zhou, A., Zhao, Y., Sun, R., Chen, J., Zheng, W., 2023. The efficiency of Hg cold vapor generation and its influence on Hg isotope analysis by MC-ICP-MS. J. Anal. At. Spectrom. https://doi.org/10.1039/d3ja00056g.
- Smart, M.S., Filippelli, G., Gilhooly III, W.P., Marshall, J.E.A., Whiteside, J.H., 2022. Enhanced terrestrial nutrient release during the Devonian emergence and expansion of forests: evidence from lacustrine phosphorus and geochemical records. GSA Bull. https://doi.org/10.1130/B36384.1.
- Song, Y., Gilleaudeau, G.J., Algeo, T.J., Over, D.J., Lyons, T.W., Anbar, A.D., Xie, S., 2021. Biomarker evidence of algal-microbial community changes linked to redox and salinity variation, Upper Devonian Chattanooga Shale (Tennessee, USA). GSA Bull. 133, 409–424.
- Stock, C.W., Sandberg, C.A., 2019. Latest Devonian (Famennian, expansa Zone) conodonts and sponge-microbe symbionts in Pinyon Peak Limestone, Star Range, southwestern Utah, lead to reevaluation of global Dasberg Event. Palaeogeogr. Palaeoclimatol. Palaeoecol. 534, 109271.
- Them, T.R., Jagoe, C.H., Caruthers, A.H., Gill, B.C., Grasby, S.E., Gröcke, D.R., Yin, R., Owens, J.D., 2019. Terrestrial sources as the primary delivery mechanism of mercury to the oceans across the Toarcian Oceanic Anoxic Event (Early Jurassic). Earth Planet. Sci. Lett. 507, 62–72.
- Thibodeau, A.M., Bergquist, B.A., 2017. Do mercury isotopes record the signature of massive volcanism in marine sedimentary records? Geology 45, 95–96.
- Thibodeau, A.M., Ritterbush, K., Yager, J.A., West, A.J., Ibarra, Y., Bottjer, D.J., Berelson, W.M., Bergquist, B.A., Corsetti, F.A., 2016. Mercury anomalies and the timing of biotic recovery following the end-Triassic mass extinction. Nat. Commun. 7, 11147
- Walliser, O.H., 1996. Global events in the Devonian and Carboniferous. In: Walliser, O.H. (Ed.), Glob. Events Event Stratigr. Phaneroz. Results Int. Interdiscip.

- Coop. IGCP-Proj. 216 "Global Biol. Events Earth Hist". Springer, Berlin, Heidelberg, pp. 225–250.
- Whiteside, J.H., Grice, K., 2016. Biomarker records associated with mass extinction events. Annu. Rev. Earth Planet. Sci. 44, 581–612.
- Williams, J.W., Shuman, B., Bartlein, P.J., 2009. Rapid responses of the prairieforest ecotone to early Holocene aridity in mid-continental North America. Glob. Planet. Change 66, 195–207.
- Xie, S., Pancost, R.D., Huang, J., Wignall, P.B., Yu, J., Tang, X., Chen, L., Huang, X., Lai, X., 2007. Changes in the global carbon cycle occurred as two episodes during the Permian–Triassic crisis. Geology 35, 1083–1086.
- Zhang, F., Dahl, T.W., Lenton, T.M., Luo, G., Shen, S., Algeo, T.J., Planavsky, N., Liu, J., Cui, Y., Qie, W., Romaniello, S.J., Anbar, A.D., 2020. Extensive marine anoxia associated with the Late Devonian Hangenberg Crisis. Earth Planet. Sci. Lett. 533, 115976.
- Zhao, H., Shen, J., Algeo, T.J., Racki, G., Chen, J., Huang, C., Song, J., Qie, W., Gong, Y., 2022. Mercury isotope evidence for regional volcanism during the Frasnian-Famennian transition. Earth Planet. Sci. Lett. 581, 117412.
- Zheng, W., Demers, J.D., Lu, X., Bergquist, B.A., Anbar, A.D., Blum, J.D., Gu, B., 2019. Mercury stable isotope fractionation during abiotic dark oxidation in the presence of thiols and natural organic matter. Environ. Sci. Technol. 53, 1853–1862.
- Zheng, W., Gilleaudeau, G.J., Kah, L.C., Anbar, A.D., 2018. Mercury isotope signatures record photic zone euxinia in the Mesoproterozoic ocean. Proc. Natl. Acad. Sci. USA 115, 10594–10599.
- Zheng, W., Hintelmann, H., 2010. Isotope fractionation of mercury during its photochemical reduction by low-molecular-weight organic compounds. J. Phys. Chem. A 114, 4246–4253.